




 Cite this: *RSC Adv.*, 2018, 8, 26423

# Electronic structure and luminescence assets in white-light emitting $\text{Ca}_2\text{V}_2\text{O}_7$ , $\text{Sr}_2\text{V}_2\text{O}_7$ and $\text{Ba}_2\text{V}_2\text{O}_7$ pyro-vanadates: X-ray absorption spectroscopy investigations

 Aditya Sharma, \* Mayora Varshney, Keun-Hwa Chae  and Sung Ok Won\*

$\text{Ca}_2\text{V}_2\text{O}_7$ ,  $\text{Sr}_2\text{V}_2\text{O}_7$ , and  $\text{Ba}_2\text{V}_2\text{O}_7$  pyro-vanadates were synthesized using a modified chemical precipitation method and annealing. Detailed crystal structure, morphology, electronic structure and optical properties were investigated by XRD, UV-visible absorption, FTIR, Raman, FE-SEM, XANES, and photoluminescence spectroscopy. Rietveld refinement on the XRD patterns of  $\text{Ca}_2\text{V}_2\text{O}_7$ ,  $\text{Sr}_2\text{V}_2\text{O}_7$ , and  $\text{Ba}_2\text{V}_2\text{O}_7$  has confirmed the triclinic structure (space group:  $\bar{P}1(2)$ ) of the pyro-vanadates. The band gap energy of  $\text{Ca}_2\text{V}_2\text{O}_7$ ,  $\text{Sr}_2\text{V}_2\text{O}_7$ , and  $\text{Ba}_2\text{V}_2\text{O}_7$  is estimated to be  $\sim 2.67$  eV,  $\sim 2.97$  eV and  $\sim 3.09$  eV, respectively. XANES spectra at the Ca L-edge, Sr K-edge and Ba L-edge have confirmed the  $\text{Ca}^{2+}$ ,  $\text{Sr}^{2+}$  and  $\text{Ba}^{2+}$  ions in the  $\text{Ca}_2\text{V}_2\text{O}_7$ ,  $\text{Sr}_2\text{V}_2\text{O}_7$  and  $\text{Ba}_2\text{V}_2\text{O}_7$  compounds, respectively. V K-edge XANES spectra have strengthened the presence of sub-pentavalent V ions in all of the pyro-vanadates. O K-edge XANES spectra of  $\text{Ca}_2\text{V}_2\text{O}_7$ ,  $\text{Sr}_2\text{V}_2\text{O}_7$  and  $\text{Ba}_2\text{V}_2\text{O}_7$  have shown dominating tetrahedral symmetry of the V ions which is also corroborated with the V K-edge XANES. Broad-band emission spectra, ranging from 400 nm to 700 nm, have been observed from the charge-transfer transitions of  $\text{VO}_4$  tetrahedra.  ${}^3\text{T}_1 \rightarrow {}^1\text{A}_1$  and  ${}^3\text{T}_2 \rightarrow {}^1\text{A}_1$  transitions, from the  $\text{VO}_4$  tetrahedra, have provided two distinct emission peaks from the compounds which exhibit a red-shift with the decreasing ionic-radii of alkali-earth metal ions. The mixed compounds, with equal weight proportions, have shown remarkable emission characteristics towards the realization of rare-earth element free white-light-emitting devices.

Received 19th April 2018

Accepted 18th July 2018

DOI: 10.1039/c8ra03347a

[rsc.li/rsc-advances](http://rsc.li/rsc-advances)

## Introduction

Analogous to the transition metal based pyro-vanadates,  $\text{M}_2\text{V}_2\text{O}_7$  (M = transition metal; Mn, Co, Ni and Cu *etc.*),<sup>1–5</sup> the alkali earth metal based  $\text{A}_2\text{V}_2\text{O}_7$  (A = Ca, Sr and Ba *etc.*) oxides are of special interest because of their promising applications in rare earth element free white-light-emitting devices<sup>6–10</sup> and microwave-dielectrics.<sup>11,12</sup>

The electron correlation effects (because of the V–O4, V–O5 and V–O6 kinds of conceivable polyhedral configuration of V and O ions) make  $\text{A}_2\text{V}_2\text{O}_7$  oxides attractive candidates for probing their intriguing correlations among the crystal structure, electronic/atomic structure and diverse applications. The alkali earth metal based pyro-vanadates (*i.e.*,  $\text{Ca}_2\text{V}_2\text{O}_7$ ,  $\text{Sr}_2\text{V}_2\text{O}_7$  and  $\text{Ba}_2\text{V}_2\text{O}_7$  *etc.*) obey the triclinic crystal structure. Their band structure, near the Fermi level, is characteristically formed by the hybridization of the frontier V d-orbitals and O 2p-orbitals. The bottom of the conduction band is shaped by the anti-bonding O 2p and V 3d orbitals and the top of the valence band mainly consists of non-bonding O 2p-orbitals.<sup>8,10</sup> The orbitals of the alkali earth elements provide a large conduction

band-width and do not contribute to the band structure near the Fermi level. The energy-band structure and, thus, the electronic/optical/magnetic properties of  $\text{A}_2\text{V}_2\text{O}_7$  oxides are not only sensitive to the amalgamation of foreign elements<sup>13–15</sup> but are also expected to be modified by the distortion in the V–O polyhedra. A marginal distortion in the metal–oxygen polyhedra can affect the hybridization between the O 2p and metal d orbitals, which indeed regulate the band structure near the Fermi level and, consequently, the electronic/optical properties of the compounds.<sup>16,17</sup>

Optical properties and illumination performance of the compounds are categorically determined by the electronic structure around the stimulated ions and energy transfer processes among them.<sup>18–22</sup> In case of vanadium-based optical materials, the  $(\text{VO}_4)^{3-}$  groups obey broad and strong charge-transfer (CT) absorption bands near the UV region and, thus, produce broad-emission spectra related to the electronic/atomic structure of the compound where the V ions are coordinated by the four O ligands.<sup>8–10,19,20</sup> In previous reports, the  $\text{Sr}_2\text{V}_2\text{O}_7$  and  $\text{Ba}_2\text{V}_2\text{O}_7$  have shown broad emission characteristics ranging from 400 nm to 700 nm and have signified the concept of vanadium-based and rare-earth-free white-light emitting phosphor materials with high efficiency.<sup>8–10,19,20</sup> However, synthesis of single phase  $\text{A}_2\text{V}_2\text{O}_7$  oxides is challenging

Advance Analysis Centre, Korea Institute of Science and Technology (KIST), Seoul-02792, South Korea. E-mail: [adityaiuac@gmail.com](mailto:adityaiuac@gmail.com); [sowon@kist.re.kr](mailto:sowon@kist.re.kr)



because of unpredictable nature of V ions to form secondary phases of  $\text{VO}_2$ ,  $\text{V}_2\text{O}_5$  etc. under the chemical and/or thermal treatment and, therefore, high-purity phase fabrication of  $\text{A}_2\text{V}_2\text{O}_7$  compounds is still a thirsty area of research for establishing the financially viable and straightforward synthesis approaches.

Besides the single-phase synthesis of  $\text{A}_2\text{V}_2\text{O}_7$  compounds, investigations on the crystal structure and electronic structure properties, which may have diverse V–O hybridization and complex electronic correlation, are also indispensable using the modern, non-destructive and element specific techniques. In this regard, X-ray photoelectron spectroscopy (XPS) had been applied to probe the electronic structure and chemical environment in pyro-vanadates.<sup>23–25</sup> The XPS is sensitive to a few surface layers of the samples and an insulating/less-conducting sample undergoes severe charging effects during the measurements. Therefore, XPS is not ideally suited to correlate the structural features to the electronic/atomic structure properties of bulk of the material. In this study, in order to investigate the relationship among the crystal structure, orbital hybridization and optical properties of  $\text{A}_2\text{V}_2\text{O}_7$  pyro-vanadates, we have systematically applied the X-ray absorption near edge structure (XANES) spectroscopy technique at O K-edge, V L-edge, Ca L-edge, Sr K-edge, V K-edge and Ba L-edge. Besides providing the detailed experimental results on the absorption edges of constituent elements of the samples, the XANES investigations presented below address the several aspects. First, to specifically look into the dissimilarities in the hybridization of frontier orbitals of V and O ions in  $\text{Ca}_2\text{V}_2\text{O}_7$ ,  $\text{Sr}_2\text{V}_2\text{O}_7$  and  $\text{Ba}_2\text{V}_2\text{O}_7$ , the low energy XANES spectra at O K-edge and V L-edge were studied. Secondly, to understand valence state of constituent elements in the samples, systematic, XANES spectra at Ca L-edge, Ba L-edge, Sr K-edge, V K-edge were collected and analyzed.

## Experimental

The analytical grade calcium nitrate ( $\text{Ca}(\text{NO}_3)_2 \cdot 4\text{H}_2\text{O}$ ), strontium nitrate ( $\text{Sr}(\text{NO}_3)_2$ ), Barium carbonate ( $\text{BaCO}_3$ ), and ammonium meta-vanadate ( $\text{NH}_4\text{VO}_3$ ) were chosen as starting reagents for the synthesis of  $\text{Ca}_2\text{V}_2\text{O}_7$ ,  $\text{Sr}_2\text{V}_2\text{O}_7$  and  $\text{Ba}_2\text{V}_2\text{O}_7$  ceramics. The stoichiometric proportions (1 : 1) were set for the alkali earth metal and vanadium precursors for preparing the  $\text{A}_2\text{V}_2\text{O}_7$  pyro-vanadates. The stoichiometric mixture of precursors was dispersed in 100 ml DI water under the sonication for 10 min. Then the solutions were stirred for 1 h with a bottom plate temperature of 100 °C. After fair dissolution of precursors, the pH of the solution was increased up to 9 by adding the  $\text{NH}_4\text{OH}$ . After increasing pH, each sample was continuously stirred for one more hour at the same temperature. The precipitates were washed with 1 L water and then filtered. The filtered cake was dried in an oven at 80 °C for overnight. Such samples were crushed in the mortar-pestle and calcined at 800 °C for 4 hours. The X-ray diffraction measurements were performed using the Dmax-2500 (Rigaku) X-ray diffractometer. This machine uses the source of Cu K $\alpha$  radiation ( $\lambda = 1.5418 \text{ \AA}$ ), operated at the voltage of 40 kV and current of 200 mA. A wide

scan range (5–140°) was scanned with the fixed time scan mode. For this 2 seconds was the fixed time for each 0.01° step. UV-visible absorption spectra were collected from the Cary500 (Agilent, US) UV-VIS-NIR spectrophotometer. This machine can produce the photon wavelength ranging from 3300 nm to 175 nm with dual beam method. Fourier-transformed infrared spectroscopy (FT-IR) measurements were performed using iS10FT-IR spectrophotometer (ThermoFisher Scientific). This instrument can provide a wide range of photon wavenumber ranging from 6500  $\text{cm}^{-1}$  to 500  $\text{cm}^{-1}$ . The Raman spectra were collected by using the Renishaw (In-Via Raman) microscope with an Nd:YAG (neodymium-doped yttrium aluminum garnet) laser, which produces a photon beam of the wavelength of 532 nm. Scanning electron microscopy measurements were performed by applying the FEI (Inspect F50), scanning electron microscope with operational voltage < 30 kV. Photoluminescence was measured using a Varian-Cary eclipse fluorescence spectrophotometer equipped with a 150 W xenon lamp as the excitation source. The low energy XANES spectra at the O K-edge, V L-edge and Ca L-edge were collected in total electron yield (TEY) mode at the soft X-rays beamline, 10D-XAS-KIST, at Pohang Accelerator Laboratory (PAL), South Korea. The photon energy resolution of this beamline was better than 0.6 eV (at the O K-edge). The high energy XANES at V K-edge, Ba L-edge, Sr K-edge were collected from the 1D XRS KIST-PAL beamline. The procedure of data collection and uses of gas-mixtures were kept similar to our previous experiments.<sup>26–28</sup>

## Results

### (a) XRD, UV-visible absorption, FTIR, Raman and FE-SEM studies

Fig. 1 shows the Rietveld refined XRD patterns of pyro-vanadate ceramics sintered at 800 °C for 4 hours. All ceramics flawlessly matched with their relevant JCPDF files; #97-002-0609, #97-007-2200 and #97-003-4320 for  $\text{Ca}_2\text{V}_2\text{O}_7$ ,  $\text{Sr}_2\text{V}_2\text{O}_7$  and  $\text{Ba}_2\text{V}_2\text{O}_7$  respectively. The initial structure models in the Rietveld refinements of a pyro-vanadate compound were taken from the respective JCPDF files. The insets of Fig. 1 show the magnified view of the simulated patterns. The crystallographic data of  $\text{Ca}_2\text{V}_2\text{O}_7$ ,  $\text{Sr}_2\text{V}_2\text{O}_7$ , and  $\text{Ba}_2\text{V}_2\text{O}_7$  is presented in Table 1. It is noticeable from the Table 1 that all three ceramics have a triclinic structure with  $P\bar{1}(2)$  space group symmetry without forming any secondary phase and, thus, are signifying the single phase formation of pyro-vanadate in this study. Moreover, the lattice parameters and cell volume are higher for the  $\text{A}_2\text{V}_2\text{O}_7$  ceramics with increasing the atomic number of the alkali earth element and are consistent with the previous reports.<sup>8–10</sup>

Fig. 2(a) shows the UV-visible absorption spectra of  $\text{Ca}_2\text{V}_2\text{O}_7$ ,  $\text{Sr}_2\text{V}_2\text{O}_7$ , and  $\text{Ba}_2\text{V}_2\text{O}_7$  samples. It is noticeable from the Fig. 2 that the  $\text{Ca}_2\text{V}_2\text{O}_7$ ,  $\text{Sr}_2\text{V}_2\text{O}_7$ , and  $\text{Ba}_2\text{V}_2\text{O}_7$  show a sharp absorption edge  $\sim 465 \text{ nm}$ ,  $\sim 418 \text{ nm}$  and  $\sim 402 \text{ nm}$ , respectively. Fig. 2(b) shows the band-gap energy estimation from the UV-visible absorption spectra. The band-gap energy was estimated by plotting the  $h\nu$  versus  $(\alpha h\nu)^2$  curves (Tauc's procedure, where  $\alpha$  is the absorption coefficient and  $h\nu$  is the photon



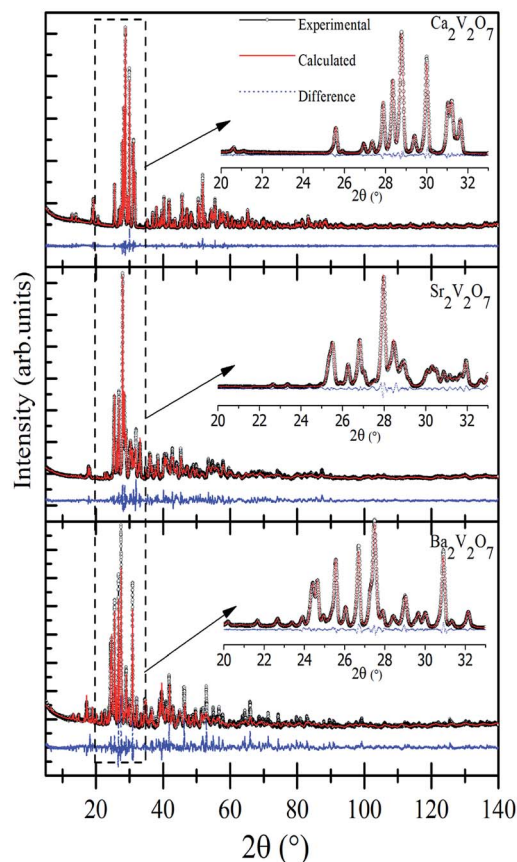


Fig. 1 Experimental and Rietveld refined XRD patterns of  $\text{Ca}_2\text{V}_2\text{O}_7$ ,  $\text{Sr}_2\text{V}_2\text{O}_7$ , and  $\text{Ba}_2\text{V}_2\text{O}_7$ . The insets show the magnified view of simulated and experimental data.

energy) and marking intersect at the energy scale. This gives band gap energy of 2.67 eV, 2.97 eV and 3.09 eV for the  $\text{Ca}_2\text{V}_2\text{O}_7$ ,  $\text{Sr}_2\text{V}_2\text{O}_7$ , and  $\text{Ba}_2\text{V}_2\text{O}_7$ , respectively. Thus the estimated band-gap energy of the compounds is comparable to the earlier reports.<sup>18,23,24</sup>

Fig. 2(c) shows the FTIR spectra of the  $\text{Ca}_2\text{V}_2\text{O}_7$ ,  $\text{Sr}_2\text{V}_2\text{O}_7$ , and  $\text{Ba}_2\text{V}_2\text{O}_7$  samples. All of the three samples show few dominating bands  $\nu_1$  ( $\sim 950\text{--}900\text{ cm}^{-1}$ ),  $\nu_2$  ( $830\text{--}810\text{ cm}^{-1}$ ),  $\nu_3$  ( $750\text{--}770\text{ cm}^{-1}$ ) and  $\nu_4$  ( $650\text{--}700\text{ cm}^{-1}$ ). These bands are mainly due

Table 1 Refinement parameters and crystallographic data of  $\text{Ca}_2\text{V}_2\text{O}_7$ ,  $\text{Sr}_2\text{V}_2\text{O}_7$ , and  $\text{Ba}_2\text{V}_2\text{O}_7$ . Numbers in parenthesis show error therein

	$\text{Ca}_2\text{V}_2\text{O}_7$	$\text{Sr}_2\text{V}_2\text{O}_7$	$\text{Ba}_2\text{V}_2\text{O}_7$
Symmetry	Triclinic	Triclinic	Triclinic
Space group	$P\bar{1}(2)$	$P\bar{1}(2)$	$P\bar{1}(2)$
$a$ (Å)	6.66766(8)	7.0980(5)	13.5675(1)
$b$ (Å)	6.92342(8)	13.0029(9)	7.3278(9)
$c$ (Å)	7.01801(8)	7.0535(5)	7.3297(9)
$\alpha$ (°)	86.4432(5)	93.725(3)	90.132(5)
$\beta$ (°)	63.8597(4)	90.750(3)	99.391(3)
$\gamma$ (°)	83.6884(5)	99.358(3)	87.314(3)
Volume (Å) <sup>3</sup>	289.042(6)	640.80(8)	718.15(15)
$R$ -Bragg (%)	2.386	1.345	1.436
$R_{\text{wp}}$ (%)	7.732	9.21	9.57
GOF	1.28	2.92	2.51

to the stretching vibrations of metal-oxygen bonds and bending vibrations of  $\text{VO}_4^{3-}$  groups in triclinic structured  $\text{A}_2\text{V}_2\text{O}_7$  pyrovanadates.<sup>29,30</sup> The  $\nu_4$  and  $\nu_3$  bands are the results of V–O–V bridge vibration and asymmetric stretching of longer V–O bond.<sup>31,32</sup> The rest of the bands ( $\nu_1$  and  $\nu_2$ ) can be ascribed to symmetric stretching of the other shorter V–O bonds in the samples.<sup>31,32</sup> Therefore, the feature-rich FTIR spectra convey the existence of  $\text{VO}_4^{3-}$  groups in all of the pyrovanadates.

Fig. 2(d) shows the Raman spectra of  $\text{Ca}_2\text{V}_2\text{O}_7$ ,  $\text{Sr}_2\text{V}_2\text{O}_7$ , and  $\text{Ba}_2\text{V}_2\text{O}_7$  samples. Similar to the FTIR spectra, the Raman spectra have shown several vibration bands of V–O bonds. In all three samples, the Raman modes can be seen within the three distinct regions. The first region is between the  $950\text{--}800\text{ cm}^{-1}$  and can be ascribed to the symmetric stretching vibrations of end  $\text{VO}_3$  groups.<sup>33–35</sup> The second region is from  $800\text{ cm}^{-1}$  to  $400\text{ cm}^{-1}$  and attributed to stretching vibrations of bridging V–O–V band bending vibrations.<sup>33–35</sup> The third region contains bands below the  $400\text{ cm}^{-1}$  and may be due to the peripheral modes.<sup>33–35</sup> Though the pyrovanadates give their rich Raman bands due to the V–O or V–O–V bonds in the samples, however, their position is sensitive to the type of alkali metal element and defect chemistry.<sup>33–35</sup>

To investigate the surface morphology of the  $\text{Ca}_2\text{V}_2\text{O}_7$ ,  $\text{Sr}_2\text{V}_2\text{O}_7$  and  $\text{Ba}_2\text{V}_2\text{O}_7$  samples, systematic FE-SEM images were collected and are presented in Fig. 3(a–c). It is noticeable from the micrographs that all pyrovanadate have unusual and agglomerated morphology. This unusual morphology may arise due to the diffusion of particles during annealing of samples.<sup>36,37</sup> The FE-SEM images ruled out the formation of fascinating morphologies (*i.e.*, nano-rod, nano-wire or other structures) and, therefore, the observed luminescence properties are expected to be related only to the electronic/atomic structure properties but not due to the diverse surface/interface related phenomena in nanostructures.

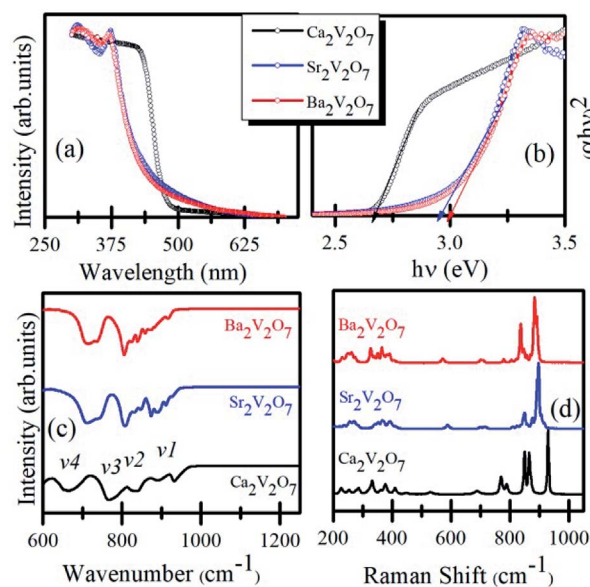


Fig. 2 (a) UV-visible absorption spectra of  $\text{Ca}_2\text{V}_2\text{O}_7$ ,  $\text{Sr}_2\text{V}_2\text{O}_7$ , and  $\text{Ba}_2\text{V}_2\text{O}_7$ . (b) Shows the Tauck's plot for determining the band-gap energy. (c) FTIR spectra. (d) Raman spectra of the samples.





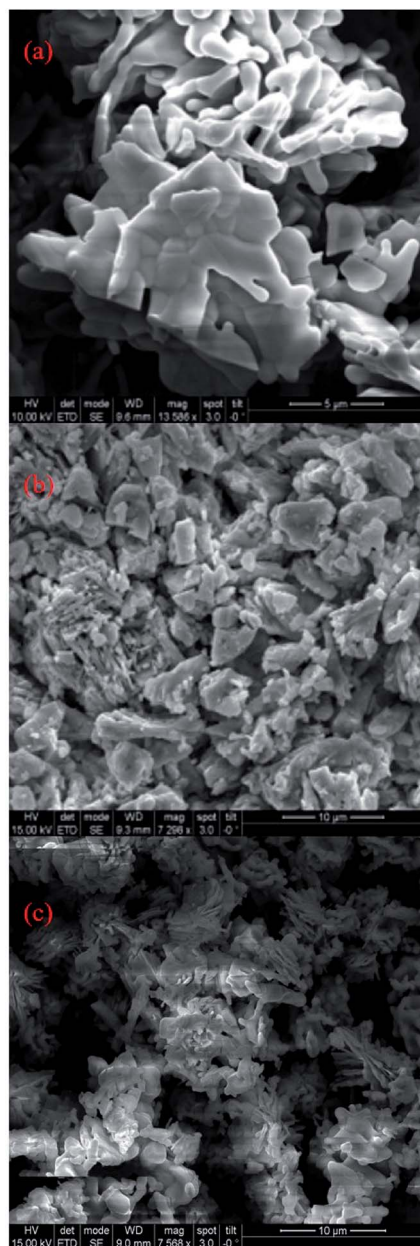


Fig. 3 FE-SEM images of (a)  $\text{Ca}_2\text{V}_2\text{O}_7$ , (b)  $\text{Sr}_2\text{V}_2\text{O}_7$  and (c)  $\text{Ba}_2\text{V}_2\text{O}_7$ .

### (b) Electronic structure study by XANES

Formation of secondary phases in the host, lattice defects and variation in the coordination chemistry of the elements may facilitate ambiguous changes in the valence state of the metal ions in the pyro-vanadates. Therefore, to understand the valence state of Ca, Sr and Ba elements in the samples XANES spectra at Ca  $L_{3,2}$ -edge, Sr K-edge and Ba  $L_{3,2}$ -edge were collected and the normalized spectra, along with first derivative spectra, are presented in the Fig. 4 (a–c). The reference samples of CaO, SrO, and BaO, in which valence state of alkali earth cations is  $2+$  (*i.e.*,  $\text{Ca}^{2+}$ ,  $\text{Sr}^{2+}$  and  $\text{Ba}^{2+}$ ), were also scanned under the similar experimental conditions and the spectra are plotted along with the  $\text{A}_2\text{V}_2\text{O}_7$  samples. It is noticeable from Fig. 4 that the edge-energy position and spectral features of reference CaO,

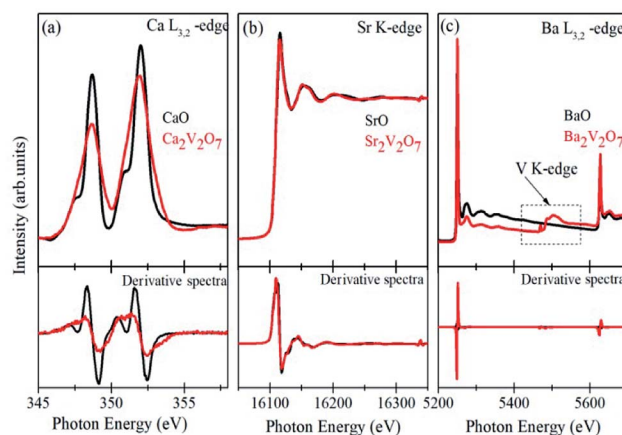


Fig. 4 (a) Ca L-edge XANES of CaO and  $\text{Ca}_2\text{V}_2\text{O}_7$  samples, (b) Sr K-edge XANES of SrO and  $\text{Sr}_2\text{V}_2\text{O}_7$  samples and (c) Ba L-edge XANES of BaO and  $\text{Ba}_2\text{V}_2\text{O}_7$  samples. Lower panels show the first derivative spectra from the respective samples.

SrO and BaO samples fairly resemble with the  $\text{Ca}_2\text{V}_2\text{O}_7$ ,  $\text{Sr}_2\text{V}_2\text{O}_7$ , and  $\text{Ba}_2\text{V}_2\text{O}_7$ , respectively, and are strengthening the  $2+$  valence state of the alkali earth cations in  $\text{A}_2\text{V}_2\text{O}_7$  pyro-vanadates of this study. Interestingly, Ba  $L_{2,3}$ -edge XANES of  $\text{Ba}_2\text{V}_2\text{O}_7$  sample shows additional spectral features between the 5400 eV to 5600 eV. V K-edge spectral features originate within this energy range.<sup>16</sup> In the present study, the existence of V ions in  $\text{Ba}_2\text{V}_2\text{O}_7$  sample is responsible for such spectral features. We have not seen any ambiguous spectral feature of secondary phases and, thus, the XANES spectra at Ca L-edge, Sr K-edge and Ba L-edge can convince the  $2+$  valence state of alkali earth elements and strengthened our XRD results of single phase nature of the samples.

Fig. 5(a) shows the pre/post-edge background subtracted and normalized V K-edge XANES spectra from the V metal foil,  $\text{VO}_2$ ,  $\text{V}_2\text{O}_5$  and  $\text{A}_2\text{V}_2\text{O}_7$  samples. The first absorption feature between 5465–5475 eV, known as pre-edge peak, originates due to the transitions from  $1s$  core levels to  $3d$  state. Although, it is a dipole-forbidden transition but originates because of the combination of strong  $3d$ – $4p$  mixing and overlap of the metal  $3d$  orbitals with the surrounding O  $2p$  orbitals.<sup>16,38,39</sup> Above the edge-energy, a strong peak is present in every spectrum which originates due to the dipole-allowed  $1s$ – $4p$  transitions followed by the other higher energy features from the transitions to higher  $np$  states and other multiple scattering contributions or, simply, the EXAFS signals.<sup>16,38,39</sup> It is noticeable from the Fig. 5(a) that reference samples show a systematic edge-energy shift towards higher energy with increasing oxidation state of the V ions (*i.e.*, energy position order is  $\text{V}_2\text{O}_5 > \text{VO}_2 > \text{V}$ ). The variation in the energy position is fairly visible from the second derivative spectra of the V K-edge XANES, presented in the Fig. 5(b) and inset therein. The edge-energy variation in the V K-edge spectra is corresponding to the oxidation state changes in the samples.

The change in valence state has been estimated, quantitatively, by plotting the relative energy position of  $1s$ – $4p$  peak to the pre-edge peak as a function of formal oxidation state *via* deriving an approximate calibration curve<sup>16,38</sup> and is presented



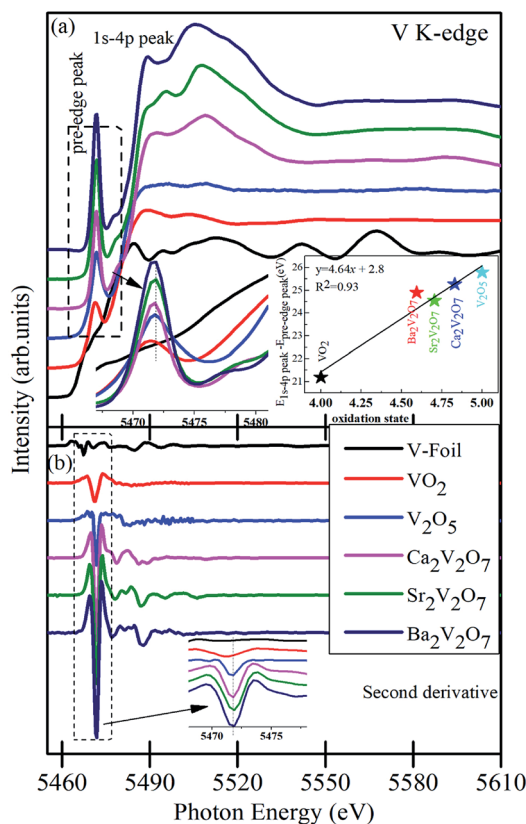


Fig. 5 (a) V K-edge XANES of V, foil,  $\text{VO}_2$  and  $\text{V}_2\text{O}_5$  reference samples along with  $\text{A}_2\text{V}_2\text{O}_7$  ceramics. (b) The second derivative of XANES spectra from the samples. The first inset of the (a) shows the magnified view of the pre-edge region and the second inset shows the oxidation state of the compounds. Inset of (b) shows the magnified view of the second derivative of XANES spectra. Spectra are vertically moved for the clarity of the presentation.

in the inset of Fig. 5(a). It is noticeable that the  $\text{A}_2\text{V}_2\text{O}_7$  samples show the sub-pentavalent state of V ions. But the oxidation state of V ions in  $\text{A}_2\text{V}_2\text{O}_7$  samples is comparable (4.62–4.82), regardless of the variation in the alkali-metal element in the compounds. A little less oxidation of V ions, than the expected 5+ oxidation, could be due to the perturbation in the oxygen stoichiometry in the  $\text{A}_2\text{V}_2\text{O}_7$  samples under the given synthesis conditions.

Besides the oxidation state estimation of V ions, the pre-edge peak is prone to the electronic configuration (or empty density of states) and local symmetry of the V ions in various compound.<sup>38,39</sup> The pre-edge intensity will be virtually zero in case of regular octahedral symmetry of the V ions but it enhances for the distorted symmetric compounds and reaches to maximum for the tetrahedral symmetric compounds.<sup>39</sup> In the present study, the pre-edge intensity of  $\text{A}_2\text{V}_2\text{O}_7$  compounds is superior to the  $\text{VO}_2$  or  $\text{V}_2\text{O}_5$  samples and is strengthening the more distorted octahedral symmetry or existence of tetrahedral symmetry of V ions in the pyro-vanadates. The  $\text{Ca}_2\text{V}_2\text{O}_7$  compound is exhibiting a lower intensity of pre-edge peak, while compared with  $\text{Sr}_2\text{V}_2\text{O}_7$  and  $\text{Ba}_2\text{V}_2\text{O}_7$ , which may indicate lesser transition probabilities from the V 1s core levels to 3d states in this compound compared with other two pyro-

vanadates. Moreover, the pre-edge intensity of V K-edge XANES spectra of  $\text{A}_2\text{V}_2\text{O}_7$  may be subjected to the diverse 3d-4p mixing and overlapping of O 2p with the V 3d orbitals under the influence of alkali metal orbitals. Therefore, to understand the local symmetry of V ions, surrounded by the O ligands in  $\text{A}_2\text{V}_2\text{O}_7$  compounds, it is advantageous to investigate the O K-edge XANES because it gives precise measure of bottom of the conduction band of a compound *via* probing the unoccupied density of states in  $t_{2g}$  and  $e_g$  orbitals along with the measure of crystal field splitting.

Fig. 6(a) and (b) present the V L-edge and O K-edge XANES spectra of  $\text{Ca}_2\text{V}_2\text{O}_7$ ,  $\text{Sr}_2\text{V}_2\text{O}_7$ , and  $\text{Ba}_2\text{V}_2\text{O}_7$  compounds. As stated above, the  $d^0$  electronic configuration of V d orbitals provides 5+ oxidation state of V ions in  $\text{A}_2\text{V}_2\text{O}_7$  compounds which is similar to the oxidation state of V ions in  $\text{V}_2\text{O}_5$  compound (*i.e.*,  $\text{V}^{5+}$ ). Therefore, spectral features and energy position of  $\text{A}_2\text{V}_2\text{O}_7$  compounds were compared with the V L-edge and O K-edge XANES spectrum of the reference  $\text{V}_2\text{O}_5$  compound.

According to the dipole selection rules ( $\Delta l = \pm 1$ ), XANES spectra at V L-edge and O K-edge are originated due to the d-projected unoccupied density of states and p-projected density of states of the valence levels, respectively.<sup>39–42</sup> There are two distinct peaks in the V L-edge spectra at  $\sim 519.5$  eV (peak c; known as  $\text{L}_{3\text{-edge}}$ ) and  $526.5$  eV (peak d; known as  $\text{L}_{2\text{-edge}}$ ), which are corresponding to the electronic transitions from the V  $2p_{3/2}$  and V  $2p_{1/2}$  core levels, respectively, to the un-occupied 3d levels.<sup>16,38–40</sup> The V  $\text{L}_3$  and  $\text{L}_2$ -edges of vanadium compounds obey several spectral features which originate from the crystal field and/or atomic-multiplet effects.<sup>39–42</sup> However, the V  $\text{L}_2$ -edge is less important for the analysis because of its broadened nature *via* the Coster–Kronig Auger decay process into a  $2p_{3/2}$  hole.<sup>39</sup> Therefore well-resolved V  $\text{L}_3$ -edge features are important to understand the electronic structure assets of the compounds. According to the band-structure calculations of vanadium

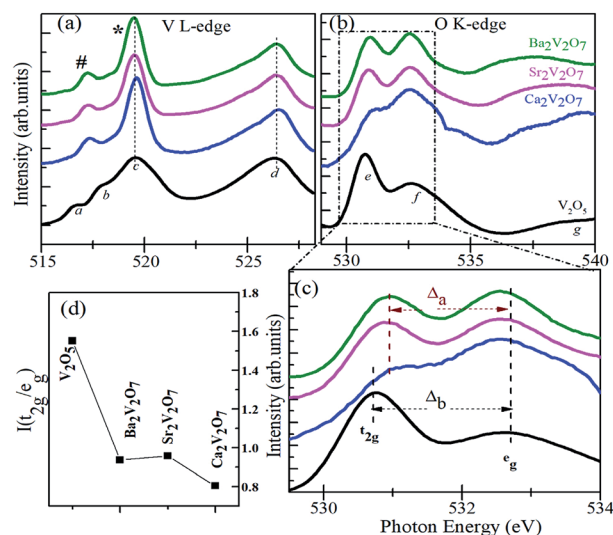


Fig. 6 V L-edge XANES spectra (a) and O K-edge XANES spectra (b) of  $\text{Ca}_2\text{V}_2\text{O}_7$ ,  $\text{Sr}_2\text{V}_2\text{O}_7$  and  $\text{Ba}_2\text{V}_2\text{O}_7$  along with the reference  $\text{VO}_2$  and  $\text{V}_2\text{O}_5$  samples. (c) Shows the crystal field splitting ( $\Delta_a$ ) for the pyro-vanadates and ( $\Delta_b$ ) for the reference vanadium oxide samples. (d) Shows intensity ratio of  $t_{2g}$  and  $e_g$  peaks.

oxides by Maganas *et al.*, the *c* feature exhibits more of the  $3d_{z^2}$  character of the V ions whereas the *b* and *a* features arise from the  $3d_{xz} + 3d_{yz}$  and  $3d_{xy}$  components, respectively.<sup>43</sup> However, better-resolved spectra of vanadium oxides have also shown another spectral feature between the *b* and *c* peaks and it was assigned to the V 2p to V  $3d_{x^2-y^2}$  transitions.<sup>39</sup> In the present study, we observed two distinct peaks in the V  $L_{3-}$ -edge spectra of  $A_2V_2O_7$  compounds (*i.e.*, # and \* peaks in the Fig. 6(a)), instead of three features in the  $V_2O_5$  sample. This indicates that V  $L_{3-}$ -edge of  $A_2V_2O_7$  compounds is composed of two main transitions between the V  $2p_{3/2}$  and 3d orbitals. The # and \* peak can be assigned to the transitions between V  $2p_{3/2} \rightarrow 3d$  (*xy*, *yz*, *xz*) orbitals and V  $2p_{3/2} \rightarrow 3d$  ( $x^2$ ,  $y^2$  and  $z^2$ ) orbitals. This presumably due to the different crystal field or multiplet effects in the sub-pentavalent  $A_2V_2O_7$  with triclinic crystal structure compared with pentavalent  $V_2O_5$  with an orthorhombic crystal structure. However, there are no measurable changes in the V  $L_{3,2}$ -edge spectral features of  $Ca_2V_2O_7$ ,  $Sr_2V_2O_7$  and  $Ba_2V_2O_7$  samples and are indicating the similar local symmetry (tetrahedral) and oxidation state of V ions as suggested by the V K-edge XANES.

The feature-rich O K-edge spectra are seen in the Fig. 6(b), which are originated from the electronic transitions from O 1s to O 2p hybridized V 3d orbitals and are known to provide valuable information on the crystal structure, local symmetry of metal ions and ligand-field effects.<sup>38–42</sup> In an octahedral environment, the metal  $e_g$  ( $d_{z^2}$ ,  $d_{x^2-y^2}$ ) orbitals are pointed directly towards the O ligands to form strongly bonded  $\sigma$  bonds with the O  $p_z$  orbital. On the other hand, the metal  $t_{2g}$  ( $d_{xy}$ ,  $d_{xz}$ ,  $d_{yz}$ ) orbitals points between the O ligands and make weak  $\pi$  bonds with the O  $p_x$  and  $p_y$  orbitals.<sup>42</sup> Consequently, the energy hierarchy of the anti-bonding orbitals is  $t_{2g} < e_g$  and their intensity ratio is 3/2 for an octahedrally coordinated compound.<sup>42</sup> In contrast to the octahedral ligand field, both the symmetries of molecular orbitals and their energy hierarchy are reversed in case of tetrahedrally coordinated compounds.<sup>42</sup> As a result of the tetrahedral interaction of ligands, the hybridized molecular orbitals are characterized by lower lying  $e_g$  ( $\pi$ -type) and higher energy-lying  $t_{2g}$  ( $\sigma$ -type) orbitals with their intensity ratio of 2/3.<sup>42</sup>

As stated above, the V ions in  $V_2O_5$  obey the distorted octahedral symmetry, therefore, the *e* and *f* peaks in the O K-edge XANES can be assigned to the  $t_{2g}$  and  $e_g$ , respectively. However, the V ions form  $(VO_4)^{3-}$  groups in  $A_2V_2O_7$  compounds with tetrahedral symmetry. Therefore, the energy hierarchy of  $t_{2g}$  and  $e_g$  peaks and their intensity ratios are expected to be reversed for the  $Ca_2V_2O_7$ ,  $Sr_2V_2O_7$  and  $Ba_2V_2O_7$  samples. It can be seen from the Fig. 6(d) that the  $I(t_{2g}/e_g)$  ratio is nearly 3/2 for the  $V_2O_5$  and is significantly lowered for the  $A_2V_2O_7$  samples. However, the  $I(t_{2g}/e_g)$  ratio for the  $A_2V_2O_7$  samples is not reached up to 2/3 (for the ideal tetrahedral symmetry). This could be due to the availability of octahedral locations to a few of the V ions in  $A_2V_2O_7$  samples along with their tetrahedral occupancy. It is noticeable that, the intensity of the second peak in Fig. 6(c) is higher for the  $Ca_2V_2O_7$  sample (which gives minimum  $I(t_{2g}/e_g)$  ratio) compared with remaining two samples of pyro-vanadates. This is indicating the much-unoccupied

density of states were available for the second peak of  $Ca_2V_2O_7$  sample compared with  $Sr_2V_2O_7$  or  $Ba_2V_2O_7$ . In the present study, the  $\Delta_a$  (crystal field splitting parameter for the pyro-vanadates) is marginally lesser than the reference  $V_2O_5$  sample ( $\Delta_b$ ). In general, the octahedral ligand field (with six O ions) gives much crystal field splitting ( $\Delta$ ) values while the tetrahedral ligand field (with four O ions) leads to lesser  $\Delta$  values to a given compound.<sup>42</sup> Therefore, the observed decrease in the  $\Delta_a$  reinforces the tetrahedral symmetry in the pyro-vanadates as suggested by the V K-edge XANES.

Overall, the V K-edge and O K-edge spectra of pyro-vanadates samples strengthened tetrahedral occupancy of the V ions. However, the  $Ca_2V_2O_7$  sample point a distinct difference in the electronic hybridization of the frontier orbitals of  $Ca_2V_2O_7$  sample compared with Sr/Ba based pyro-vanadates. This could be due to the dissimilar distribution of V ions at tetrahedral/octahedral sites and their hybridization with O 2p orbitals in this compound (compared with other two pyro-vanadate).

### (c) Photoluminescence study

Fig. 7(a–c) shows the PL spectra of  $Ca_2V_2O_7$ ,  $Sr_2V_2O_7$  and  $Ba_2V_2O_7$  samples along with their CIE diagrams (g). Fig. 7(d–f) show the

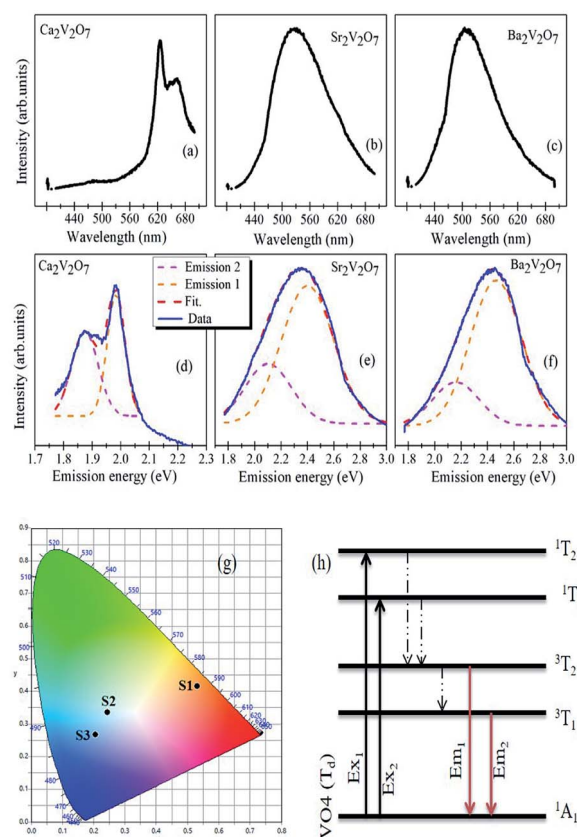


Fig. 7 (a–c) Emission spectra ( $\lambda_{ex} = 375$  nm) of  $A_2V_2O_7$  samples. (d–f) shows the deconvolution of the emission-energy spectra with two Gaussian peaks related to the two distinct emission bands from the samples. (g) Show the CIE diagram for S1 ( $Ca_2V_2O_7$ ), S2 ( $Sr_2V_2O_7$ ) and S3 ( $Ba_2V_2O_7$ ) samples. (h) Schematic for the absorption and emission characteristics of  $VO_4$  tetrahedron with  $T_d$  symmetry in pyro-vanadates.





emission spectra with the Gaussian fittings of emission bands (at energy axis). It is noticeable from the Fig. 8(a) that the  $\text{Ca}_2\text{V}_2\text{O}_7$  shows the intense emission bands near to the yellow-orange color (see spot S1 in CIE diagram) and in accordance with the previous reports.<sup>7–10</sup> The broad emission band centered  $\sim 530$  nm and  $\sim 507$  nm is observed for the  $\text{Sr}_2\text{V}_2\text{O}_7$  (Fig. 7(b)) and  $\text{Ba}_2\text{V}_2\text{O}_7$  (Fig. 7(c)) samples, respectively. This kinds of PL spectra have resulted in the blue-green and blue-indigo emission characteristic in the CIE diagram (Fig. 7g) of  $\text{Sr}_2\text{V}_2\text{O}_7$  (S2) and  $\text{Ba}_2\text{V}_2\text{O}_7$  (S3) samples, respectively.

One of the possibilities of broad-emission spectra could be the CT of an electron from O 2p orbitals to the vacant 3d orbitals of  $\text{V}^{5+}$  ions under the tetragonal symmetry of V–O4 groups.<sup>7–10</sup> In previous reports, it was also assumed that the forbidden luminescence process with the perfect tetragonal symmetry of V–O4 groups would be partially allowed due to the distorted structure as well as the spin-orbit interaction.<sup>8,10</sup> In addition to that, theoretical calculations were also performed to explain the broad emission spectra of  $\text{Sr}_2\text{V}_2\text{O}_7\text{:Eu}$  crystals.<sup>44</sup> In such calculations, a  $10 \times 10$  energy matrix was successfully established, based on an effective operator Hamiltonian, including free ion and crystal field interactions. According to the crystal field theory, the pentavalent vanadium (*i.e.*  $\text{V}^{5+}$  ions with  $3d^0$  electronic configuration) in the alkali earth metal based pyro-vanadates may not result in any d–d transitions. The d–d electronic transition based emission-characteristics can be achieved from the  $\text{V}^{5+}$  ion if it gets one electron from the surrounding oxygen atoms and attains  $3d^1$  electronic configuration *via* formation of  $\text{V}^{4+}$  ions (*i.e.*,  $\text{V}^{5+}\text{O}_4^{2-} \rightarrow \text{V}^{4+}\text{O}_4^{2-}$  (ref. 44)). Based on the theoretical calculations, it was conveyed that the broad PL properties of  $\text{Sr}_2\text{V}_2\text{O}_7\text{:Eu}$  compound originate from four different  $\text{VO}_4$  groups with  $C_{3v}$  symmetry and not from the f–d transitions of the  $\text{Eu}^{2+}$  ions. In contrary to this, f–

d transition induced broad luminescence has previously reported for the  $\text{Eu}^{3+}$  and  $\text{Eu}^{2+}$  dual emission centers.<sup>45</sup> Thus, the mechanistic concept of the broad luminescence spectra from alkali earth metal based pyro-vanadates is still under development.

In the present study, all of the samples have exhibited broad PL properties which can be assigned to the charge transfer (CT) transitions from the O 2p orbitals to the V 3d orbitals within the  $\text{VO}_4$  tetrahedra.<sup>8,10</sup> The molecular orbitals of the  $\text{V}^{5+}$  ions, with the tetrahedral symmetry, obey  $^1\text{A}_1$  ground state and four ( $^3\text{T}_1$ ,  $^3\text{T}_2$ ,  $^1\text{T}_1$  and  $^1\text{T}_2$ ) excited states as shown in the Fig. 8(h).<sup>8,10</sup> Though the all three pyro-vanadates of this study obeyed the triclinic crystal structure, with a space group of  $\text{P}\bar{1}(2)$ , there are local structural dissimilarities. In the  $\text{Ca}_2\text{V}_2\text{O}_7$ ,  $\text{VO}_4$  dimers approach to each other within the shorten unit cell (compared with the  $\text{Sr}_2\text{V}_2\text{O}_7$  and  $\text{Ba}_2\text{V}_2\text{O}_7$ ) and the  $\text{VO}_5$  pyramids are formed by the manifestation of edge-sharing at adjacent  $\text{VO}_4$  tetrahedra.<sup>8,10</sup> Therefore miscellaneous CT transitions are expected for the  $\text{Ca}_2\text{V}_2\text{O}_7$  compound which, indeed, facilitate yellow-orange emission properties. However, this kind of emission from the  $\text{A}_2\text{V}_2\text{O}_7$  needs electronic structure correlations.

In case of  $\text{A}_2\text{V}_2\text{O}_7$  compounds, the valence band is derived from the fully occupied O 2p orbitals and the conduction band is mainly consist of empty V 3d orbitals. The O K-edge XANES of  $\text{Sr}_2\text{V}_2\text{O}_7$  and  $\text{Ba}_2\text{V}_2\text{O}_7$  samples has shown similar crystal field splitting and nearly the same  $t_{2g}/e_g$  ratio which indicates iso-structured electronic structure properties in these two compound. On the other hand, the  $t_{2g}/e_g$  ratio is significantly decreased for the  $\text{Ca}_2\text{V}_2\text{O}_7$  sample. This indicates that more unoccupied 3d density of states were made available for this compound and could be due to the mixed occupancy of V ions (tetrahedral and/or octahedral). The adverse charge-transfer of an electron from O 2p orbitals to the vacant 3d orbitals of V ions under the distorted tetragonal symmetry may obey the distinct emission properties from the  $\text{Ca}_2\text{V}_2\text{O}_7$ . The diverse splitting of V 3d orbitals had previously studied for the  $\text{Ca}_2\text{V}_2\text{O}_7$  (but not seen for the  $\text{Sr}_2\text{V}_2\text{O}_7$  and  $\text{Ba}_2\text{V}_2\text{O}_7$ ) by the partial density of state (PDOS) calculations<sup>18</sup> and supports our XANES investigation.

The broad emission from the  $\text{A}_2\text{V}_2\text{O}_7$  compounds consist of two distinct emission peaks (higher energy peak (emission 1) and lower energy peak (emission 2)) which are corresponding to the transitions from  $^3\text{T}_2$  and  $^3\text{T}_1$  to the ground state  $^1\text{A}_1$  (see Fig. 7(h)). It is evident from the Fig. 7(d–f) that the emission 1 is stronger than the emission 2 and consistent of the previous reports.<sup>8,10,18</sup> Moreover, the peak position of emission 1 and emission 2 was red-shifted with decreasing the ionic radii of alkali earth ions. The luminescent colour coordinates of  $\text{A}_2\text{V}_2\text{O}_7$ , which were obtained from the CIE chromaticity diagram, were changed from yellow-orange ( $x = 0.5308$ ,  $y = 0.4151$ ; for  $\text{Ca}_2\text{V}_2\text{O}_7$ ), green-blue ( $x = 0.2445$ ,  $y = 0.3357$ ; for  $\text{Sr}_2\text{V}_2\text{O}_7$ ) to blue-indigo ( $x = 0.2053$ ,  $y = 0.2666$ ; for  $\text{Ba}_2\text{V}_2\text{O}_7$ ). The variation in the color coordination in  $\text{A}_2\text{V}_2\text{O}_7$  compounds could be due to the dissimilarities in the electronic/atomic structure as discussed above. In the present study, the CIE coordinates of  $\text{Sr}_2\text{V}_2\text{O}_7$  are quite close to the CEI coordinate of white light (*i.e.*,  $x = 0.333$ ,  $y = 0.333$ ). Moreover, advanced emission characteristics may be anticipated by mixing  $\text{A}_2\text{V}_2\text{O}_7$  pyro-vanadates in certain weight/molar ratio and has been

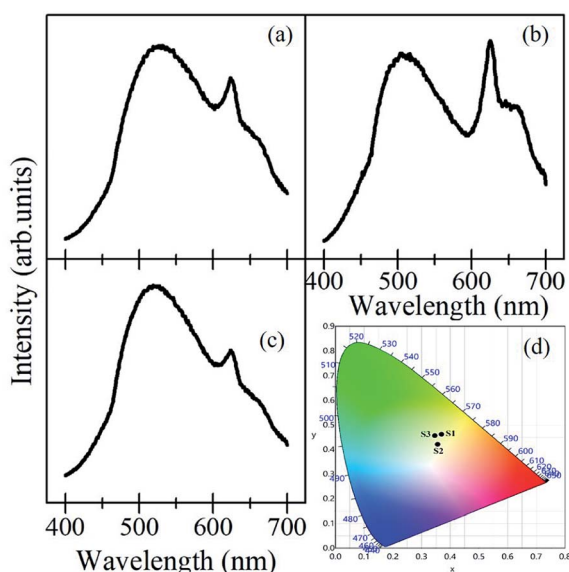


**Fig. 8** Emission spectra ( $\lambda_{\text{ex}} = 375$  nm) of mixed  $\text{A}_2\text{V}_2\text{O}_7$  samples with their equal weight proportions; (a)  $\text{Ca}_2\text{V}_2\text{O}_7 + \text{Sr}_2\text{V}_2\text{O}_7$ , (b)  $\text{Ca}_2\text{V}_2\text{O}_7 + \text{Ba}_2\text{V}_2\text{O}_7$ , (c)  $\text{Ca}_2\text{V}_2\text{O}_7 + \text{Sr}_2\text{V}_2\text{O}_7 + \text{Ba}_2\text{V}_2\text{O}_7$ . (d) Shows the CIE diagram for S1 ( $\text{Ca}_2\text{V}_2\text{O}_7 + \text{Sr}_2\text{V}_2\text{O}_7$ ), S2 ( $\text{Ca}_2\text{V}_2\text{O}_7 + \text{Ba}_2\text{V}_2\text{O}_7$ ) and S3 ( $\text{Ca}_2\text{V}_2\text{O}_7 + \text{Sr}_2\text{V}_2\text{O}_7 + \text{Ba}_2\text{V}_2\text{O}_7$ ) samples.



attempted in the present study by mixing the individual powders in their equal weight percentage.

Fig. 8(a–c) show the PL emission spectra from the mixture of the samples ((a);  $\text{Ca}_2\text{V}_2\text{O}_7 + \text{Sr}_2\text{V}_2\text{O}_7$ , (b);  $\text{Ca}_2\text{V}_2\text{O}_7 + \text{Ba}_2\text{V}_2\text{O}_7$ , and (c);  $\text{Ca}_2\text{V}_2\text{O}_7 + \text{Sr}_2\text{V}_2\text{O}_7 + \text{Ba}_2\text{V}_2\text{O}_7$ ) along with their CIE coordinate diagram in Fig. 8(d). It is evidenced from the Fig. 8 that the mixed samples have exhibited much fascinating spectral features and contain the emission bands from constituent compounds. It is noticeable that the intensity of 600 nm–700 nm peaks, which is characteristic yellow-orange emission of  $\text{Ca}_2\text{V}_2\text{O}_7$ , is significant in case of the mixture of  $\text{Ca}_2\text{V}_2\text{O}_7 + \text{Ba}_2\text{V}_2\text{O}_7$  sample but has been less dominating in case of other two combinations. This could be due to the superior emission of  $\text{Ca}_2\text{V}_2\text{O}_7$  over the  $\text{Ba}_2\text{V}_2\text{O}_7$  sample. In the Fig. 8(d), samples are named as S1 (for  $\text{Ca}_2\text{V}_2\text{O}_7 + \text{Sr}_2\text{V}_2\text{O}_7$  mixture) S2 (for  $\text{Ca}_2\text{V}_2\text{O}_7 + \text{Ba}_2\text{V}_2\text{O}_7$  mixture) and S3 (for  $\text{Ca}_2\text{V}_2\text{O}_7 + \text{Sr}_2\text{V}_2\text{O}_7 + \text{Ba}_2\text{V}_2\text{O}_7$  mixture). Thus the obtained CIE colour coordinates for S1 ( $x = 0.3696$ ,  $y = 0.4617$ ), S2 ( $0.3561$ ,  $y = 0.4207$ ) and S3 ( $0.3462$ ,  $y = 0.4562$ ) are quite diverse to that of single component pyro-vanadates. The obtained colour coordinates from the mixed compounds are very close to the white-light colour coordinates. Therefore, we may conclude that the vanadium-based compounds of the present study are proficient for the white-light-emitting devices without adding the rare-earth or other dopants.

## Conclusions

Single phase pyro-vanadate ( $\text{Ca}_2\text{V}_2\text{O}_7$ ,  $\text{Sr}_2\text{V}_2\text{O}_7$ , and  $\text{Ba}_2\text{V}_2\text{O}_7$ ) ceramics were successfully synthesized using a modified chemical precipitation method followed by air annealing of the samples.  $\text{Ca}^{2+}$ ,  $\text{Sr}^{2+}$ , and  $\text{Ba}^{2+}$  ions were confirmed in the  $\text{Ca}_2\text{V}_2\text{O}_7$ ,  $\text{Sr}_2\text{V}_2\text{O}_7$  and  $\text{Ba}_2\text{V}_2\text{O}_7$  samples, respectively, using the XANES study at the Ca L-edge, Sr K-edge and Ba L-edge. Sub-pentavalent vanadium ions have been confirmed in all three pyro-vanadates of this study by analyzing the V K-edge XANES spectra. O K-edge and V K-edge XANES have confirmed the tetrahedral occupancy in the pyro-vanadate samples. However, the  $\text{Ca}_2\text{V}_2\text{O}_7$  exhibits a smaller  $t_{2g}/e_g$  peak intensity ratio in the O K-edge which indicates a much-unoccupied density of states in O 2p and V 3d hybridized orbitals under the mixed tetrahedral/octahedral V locations in this sample. Charge-transfer transitions in  $\text{VO}_4$  tetrahedra have established broad photoluminescence characteristics in pyro-vanadates. Yellow-orange (CEI colour coordinates;  $x = 0.5308$ ,  $y = 0.4151$ ), green-blue (CEI colour coordinates;  $x = 0.2445$ ,  $y = 0.3357$ ) and blue-indigo (CEI colour coordinates;  $x = 0.2053$ ,  $y = 0.2666$ ) emissions have been observed from the  $\text{Ca}_2\text{V}_2\text{O}_7$ ,  $\text{Sr}_2\text{V}_2\text{O}_7$  and  $\text{Ba}_2\text{V}_2\text{O}_7$  samples, respectively. The emitted colour coordinates could be tailored by mixing of the compounds and has resulted in advanced photoluminescence properties which are comprehensively suitable for the rare-earth element free white-light-emitting devices.

## Conflicts of interest

There are no conflicts to declare.

## Acknowledgements

This work was supported by Korea Institute of Science and Technology, Seoul, Korea (KIST Project nos. 2V04081 and 2V04611). Authors are also thankful to Dr Jitendra Pal Singh (KIST-PAL beamline at Pohang Accelerator Laboratory, South Korea) and Dr Ankush Vij (Department of Physics, Amity University, Gurgaon, India) for fruitful discussion on EXAFS and PL data analysis.

## Notes and references

- 1 Z. He and Y. Ueda, *Phys. Rev. B: Condens. Matter Mater. Phys.*, 2008, **77**, 052402.
- 2 Z. He, J. Yamaura, Y. Ueda and W. Cheng, *Phys. Rev. B: Condens. Matter Mater. Phys.*, 2009, **79**, 092404.
- 3 S. Zhou, J. Wang, Y. Weng, Z. Wu, Z. Ni, Q. Xu, J. Du and S. Dong, *ACS Appl. Mater. Interfaces*, 2016, **8**, 26213.
- 4 M. V. Rotermel, A. Yu. Suntsova, T. I. Krasnenko, R. F. Samigullin and E. D. Pletnev, *Bull. Russ. Acad. Sci.: Phys.*, 2016, **80**, 668.
- 5 J. Wang, J. Pei, K. Hua, D. Chen, Y. Jiao, Y. Hu and G. Chen, *ChemElectroChem*, 2018, **5**, 737.
- 6 S. K. Gupta, K. Sudarshan and R. M. Kadam, *Mater. Des.*, 2017, **130**, 208.
- 7 S.-P. Kuang, Y. Meng, J. Liu, Z.-C. Wu and L.-S. Zhao, *Optik*, 2013, **124**, 5517–5519.
- 8 T. Nakajima, M. Isobe, T. Tsuchiya, Y. Ueda and T. Kumagai, *Nat. Mater.*, 2008, **7**, 735.
- 9 Y. Matsushima, T. Koide, M. H. Oka, M. Shida, A. Sato, S. Sugiyama and M. Ito, *J. Am. Ceram. Soc.*, 2015, **98**, 1236.
- 10 T. Nakajima, M. Isobe, T. Tsuchiya, Y. Ueda and T. Manabe, *J. Phys. Chem. C*, 2010, **114**, 5160.
- 11 M.-R. Joung, J.-S. Kim, M.-E. Song, S. Nahmw and J.-H. Paik, *J. Am. Ceram. Soc.*, 2009, **92**, 3092.
- 12 M.-R. Joung, J.-S. Kim, M.-E. Song, S. Nahmw, J.-H. Paik and B.-H. Choi, *J. Am. Ceram. Soc.*, 2009, **92**, 1621.
- 13 F. Li, H. Fang and Y. Chen, *J. Rare Earths*, 2017, **35**, 135.
- 14 V. Kumar, A. K. Bedyal, J. Sharma, V. Kumar, O. M. Ntwaeaborwa and H. C. Swart, *Appl. Phys. A*, 2014, **116**, 1785.
- 15 J. Gu and B. Yan, *J. Alloys Compd.*, 2009, **476**, 619.
- 16 A. Sharma, M. Varshney, W. C. Lim, H. J. Shin, J. P. Singh, S. O. Won and K. H. Chae, *Phys. Chem. Chem. Phys.*, 2017, **19**, 6397.
- 17 A. Sharma, M. Varshney, H. J. Shin, K. H. Chae and S. O. Won, *RSC Adv.*, 2017, **7**, 52543.
- 18 R. Yu, M. Yuan, T. Li, Q. Tu and J. Wang, *RSC Adv.*, 2016, **6**, 90711.
- 19 M. Takahashi, M. Hagiwara and S. Fujihara, *Inorg. Chem.*, 2016, **55**, 7879.
- 20 T. Nakajima, M. Isobe, T. Tsuchiya, Y. Ueda and T. Manabe, *Opt. Mater.*, 2010, **32**, 1618.
- 21 H. Fang, X. Wei, S. Zhou, Y. Chen, C. Duan and M. Yin, *Inorg. Chem.*, 2016, **55**, 9284.
- 22 W. Guo, W. D. Chemelewski, O. Mabayoje, P. Xiao, Y. Zhang and C. B. Mullins, *J. Phys. Chem. C*, 2015, **119**, 27220.





- 23 R. Karthik, J. V. Kumar, S.-M. Chen, P. S. Kumar, V. Selvam and V. Muthuraj, *Sci. Rep.*, 2017, **7**, 7254.
- 24 R. Yu, N. Xue, S. Huo, J. Li and J. Wang, *RSC Adv.*, 2015, **5**, 63502.
- 25 Y. Sun, J. Wang, M. Chen, C. Li, Z. Hu and S.-L. Chou, *J. Mater. Chem. C*, 2017, **5**, 6336.
- 26 A. Sharma, M. Varshney, H. J. Shin, K. H. Chae and S. O. Won, *Spectrochim. Acta, Part A*, 2017, **173**, 549.
- 27 A. Sharma, M. Varshney, H. J. Shin, K. H. Chae and S. O. Won, *Curr. Appl. Phys.*, 2016, **16**, 1342.
- 28 A. Sharma, M. Varshney, J. Park, T. K. Ha, K. H. Chae and H. J. Shin, *Phys. Chem. Chem. Phys.*, 2015, **17**, 30065.
- 29 A. C. Dhaussy, F. Abraham, O. Mentre and H. Steinfink, *J. Solid State Chem.*, 1996, **126**, 328.
- 30 I. O. Mazali and O. L. Alves, *J. Braz. Chem. Soc.*, 2004, **4**, 464.
- 31 V. B. Taxak, S. Dayawati and S. P. Khatkar, *Curr. Appl. Phys.*, 2013, **13**, 594.
- 32 H. Pan, L. Zhang, L. Jin, B. Zhang and W. Yang, *J. Electron. Mater.*, 2015, **44**, 3465.
- 33 A. N. Unnimaya, E. K. Suresh, J. Dhanya and R. Ratheesh, *J. Mater. Sci.: Mater. Electron.*, 2014, **25**, 1127.
- 34 M. L. Occelli, R. S. Maxwell and H. Eckert, *Microporous Mater.*, 1994, **3**, 305.
- 35 M. Aureliano, C. A. Ohlin, M. O. Vieira, M. Paula, M. Marques, W. H. Caseye and L. A. E. Batista de Carvalho, *Dalton Trans.*, 2016, **45**, 7391.
- 36 F. Ravoux, N. S. Rajput, J. Abed, L. George, M. Tiner and M. Jouiad, *RSC Adv.*, 2017, **7**, 32087.
- 37 N. T. H. An, M. T. Islam, J. M. Park, Y.-S. Gal, K. P. Johnston and K. T. Lim, *Mater. Lett.*, 2012, **75**, 111.
- 38 Y. Wu, L. Fan, W. Huang, S. Chen, S. Chen, F. Chen, C. Zou and Z. Wu, *Phys. Chem. Chem. Phys.*, 2014, **16**, 17705.
- 39 Y. R. Lu, H. H. Hsu, J. L. Chen, H. W. Chang, C. L. Chen, W. C. Chou and C. L. Dong, *Phys. Chem. Chem. Phys.*, 2016, **18**, 5203.
- 40 S. Zhang, B. Shang, J. Yang, W. Yan, S. Wei and Y. Xie, *Phys. Chem. Chem. Phys.*, 2011, **13**, 15873.
- 41 C. Zou, L. Fan, R. Chen, X. Yan, W. Yan, G. Pan, Z. Wu and W. Gao, *CrystEngComm*, 2012, **14**, 631.
- 42 J. G. Chen, *Surf. Sci. Rep.*, 1997, **30**, 1–152.
- 43 D. Maganas, M. Roemelt, M. Havecker, A. Trunschke, A. K. Gericke, R. Schlogl and F. Neese, *Phys. Chem. Chem. Phys.*, 2013, **15**, 7260.
- 44 W.-Q. Yang, H.-G. Liu, M. Gao, Y. Bai, J.-T. Zhao, X.-D. Xu, B. Wua, W.-C. Zheng, G.-K. Liu and Y. Lin, *Acta Mater.*, 2013, **61**, 5096.
- 45 D. K. Patel, A. Sengupta, B. Vishwanadh, V. Sudarsan, R. K. Vatsa, R. Kadam and S. K. Kulshreshtha, *Eur. J. Inorg. Chem.*, 2012, 1609.

